CrystEngComm

Accepted Manuscript

Template-free and non-hydrothermal synthesis of CeO_2 nanosheets via a facile aqueous-phase precipitation route and catalytic oxidation properties

Qiguang Dai[a]*, Shuxing Bai[a], Hua Li[b], Wei Liu[b], Xingyi Wang[a]*, Guanzhong Lu[a]

[a] Key Laboratory for Advanced Materials, Research Institute of Industrial Catalysis, East China University of Science and Technology, Shanghai 200237, PR China

[b] Key Laboratory of Nuclear Radiation and Nuclear Energy Technology, Shanghai Institute of Applied Physics, Chinese Academy of Science, Shanghai 201800, PR China

* Corresponding authors

Fax: (+86) + 21 64253372;

E-mail: daiqg@ecust.edu.cn (Q. Dai), wangxy@ecust.edu.cn (X. Wang)

ABSTRACT

Two types of CeO_2 nanosheets, petal-like and belt-like, were synthesized via a facile aqueous phase precipitation method and NH_4HCO_3 as precipitant at 0 °C and 25 °C, without hydrothermal or solvothermal treatment, without template or surfactant and without organic solvent. The reaction temperature and supersaturation played key roles in the formation of ceria nanosheets, namely, lower temperature and higher supersaturation were favorable to the synthesis of sheet-like CeO_2 by oriented aggregation of as-synthesized precursors nanocrystallines, whereas the elevated temperature could cause the dissolution-recrystallization of precursors and promote

the Ostwald ripening process, finally the polyhedral CeO_2 could be obtained through the thermal decomposition of precursors. Catalytic oxidation properties were investigated via catalytic oxidation of CO over CeO_2 and catalytic combustion of 1, 2-dichloroethane over VO_x/CeO_2. Compared with traditional CeO_2 nanoparticles, the ceria nanosheets showed more excellent catalytic oxidation activities.

KEYWORDS: CeO_2, nanosheets, catalytic oxidation, carbon monoxide, 1, 2-dichloroethane, vanadia

1. INTRODUCTION

Ceria has been widely used in catalysis, solid oxide fuel cells, oxygen sensors, ultraviolet blockers and chemical mechanical planarization processes, thus attracted tremendous attention. Over last years, remarkable progresses have been made in the synthesis of CeO_2 nanomaterials with various morphologies, such as nanorods [1], nanowires [2], nanotubes [3], nanoshuttles [4], nanoflowers [5] and other morphologies [6, 7], and in the investigation of their corresponding novel properties. Since the graphene was discovered in 2004 [8] and awarded the Nobel Prize in Physics in 2010, much more consideration has been given to synthesize metal oxides with two-dimensional (2D) nanostructures (such as nanoplates, nanodisks, nanoprisms, nanowalls, nanobelts and nanosheets) and investigate their novel applications, due to their unusual properties derived from exceptionally small thickness and possible quantum size effects [9]. However, it is difficult to synthesize 2D nanomaterials in

solution-phase, especially the material with face centered cubic structure (for example CeO_2), because there is no intrinsic driving force to form anisotropic morphology. Therefore, few previous publications have reported the synthesis of 2D CeO_2, especially CeO_2 nanosheets.

Generally, CeO_2 nanosheets are synthesized under hydrothermal or solvothermal condition and these protocols usually require templates and surfactants or the specifical precursors such as $CeOHCO_3$, and $Ce_2(CO_3)_3$, due to CeO_2 with the cubic structure. Li [10] reported the fabrication of CeO_2 nanosheets via controlling the morphology of $CeOHCO_3$ precursors by a facile hydrothermal technique in the presence of hexamethylenetetramine (HMT) and acetic acid, and their results revealed that the amount of acetic acid was a key parameter for the nucleation and crystal growth of $CeOHCO_3$ nanosheets. Yu [11] synthesized ultrathin mesoporous single-crystal-like CeO_2 nanosheets by a two-step hydrothermal treatment method. They firstly prepared Ce-EDA inorganic-organic hybrid nanorods via the hydrothermal reaction of $Ce(OAc)_3$ and 1,2-ethanediamine (EDA) at 150 °C, and then the hybrid nanorods were further hydrothermally treated at 280 °C to form nanosheets. Deng [12] successfully synthesized platelet-like CeO_2 mesocrystals, constituted of 4-5 nm fused nanoparticles with interparticular voids along a common [002] axis through a benzyl alcohol-assisted solvothermal synthesis. Among these methods, the addition of templates, surfactants or organic solvent and high temperature were necessary. In recent years, without the assistance of any surfactant or template, CeO_2 nanosheets also were successively synthesized. For examples, Liu [13] synthesized CeO_2

nanosheets with (110) dominated surface via a facile one step hydrothermal method (220 °C) and NH_3•H_2O was used to tailor the surface structure; Rao [14] described the preparation of mesoporous CeO_2 nanobelts by a hydrothermal route (120-140 °C) via only controlling cationic type (K^+, Na^+ or NH_4^+) and concentration of alkali, and the synthesized CeO_2 showed superior catalytic performance for CO oxidation; Sun [15] synthesized three-atom-thick ultrathin CeO_2 sheets with 20% surface pits at 180 °C via sodium oleate, $CeCl_3$ and NH_3•H_2O as starting materials. What was more, Yu [16] reported a simple, aqueous route to the synthesis of ultrathin, single-crystalline ceria nanosheets under non-hydrothermal condition of 95 °C, and the synthetic protocol involves the slow, continuous addition of cerium (III) nitrate into an aqueous solution containing 6-aminohexanoic acid (AHA). They found that the ceria nanosheets were formed through 2D self-organization of initially formed small ceria nanocrystals, followed by an in situ recrystallization process. Unfortunately, the template still was vital for their method. Besides, Minamidate [17], Han [18] and Wang [19] also reported the synthesis of plate-like ceria, monodisperse CeO_2 octahedra assembled by nanosheets and water-soluble Au-CeO_2 hybrid nanosheets by different methods. However, among reported methods, the requires of hydrothermal conditions (even the temperature up to 280 °C) or templates, surfactants or other organic additives, which made that the mechanism was not well understood and the post-treatment was difficult and complicated. Therefore, the synthesis of two-dimensional CeO_2 in a mild condition was still a great challenge.

Here we describe a simple, aqueous route to the synthesis of two-dimensional CeO_2

with petal and belt-like structure, without hydrothermal/solvothermal treatment, without templates and surfactants, without organic solvent and additive. Our simple synthetic protocol involves the quick addition of ammonium bicarbonate solution into cerium (III) nitrate solution at lower temperature (such as 0 °C and 25 °C). Moreover, catalytic activities of synthesized CeO_2 and VO_x/CeO_2 for the CO catalytic oxidation and 1, 2-dichloroethane catalytic combustion are investigated.

2. EXPERIMENTAL SECTION

2.1. Synthesis of CeO_2 nanosheets

In a typical synthesis procedure, 1.39 g cerium (III) nitrate hexahydrate ($Ce(NO_3)_3 \cdot 6H_2O$) and 0.75 g ammonium bicarbonate (NH_4HCO_3) were dissolved in 200 ml deionized water at 0 °C under magnetic stirring, respectively. After completely dissolved, the NH_4HCO_3 solution was poured rapidly into the $Ce(NO_3)_3$ solution, and then stirring for 0.5 h and statically aging 15 h at 0 °C. The final product was collected by filtration, washed with deionized water to remove any possible ionic remnants, and then dried at 110 °C and calcined at 450 °C for 4 h in air to prepare the petal-like CeO_2 nanosheet (labeled as CeO_2-0). To obtain different morphological CeO_2, the reaction/aging temperature and aging time were varied from 25 °C to 170 °C and 0 h to 48 h, respectively. Noting that, when the reaction/aging temperature was 75 °C and 100 °C, the reaction and aging processes were carried under reflux condition, and 150 °C and 170 °C were carried under hydrothermal condition. As reference, the CeO_2 particles (marked as CeO_2-TD) were prepared by the thermal

decomposition of $Ce(NO_3)_3 \cdot 6H_2O$ at 450 °C in air.

Vanadia was deposited on the ceria supports using incipient wetness of an aqueous solution of ammonium metavanadate (NH_4VO_3) and oxalic acid ($C_2O_4H_2$) in a 1:2 molar ratio. The concentration of vanadate and the amount of impregnation solution was adjusted in order to produce catalysts with 5 wt% vanadia weight loadings. After impregnation of the vanadate, the samples were dried overnight at 60 °C and then calcined in air at 450 °C for 4 h.

2.2. Characterization

The powder X-ray diffraction patterns (XRD) of samples were recorded on a Rigaku D/Max-rC powder diffractometer using Cu Ka radiation (40 kV and 100 mA). Scanning electron microscopy (SEM) experiments were performed on Hitachi S-3400N electron microscopes. The transmission electron microscope (TEM) images of the powder samples were recorded on a JEM-1400 instrument operated at 120 kV, and the high resolution TEM (HRTEM) images were recorded on a JEM-2100 instrument operated at 200 kV. The Fourier transform infrared spectroscopy (FT-IR) were obtained on a Nicolet 6700, and the samples were ground with KBr and pressed into thin wafer.

The H_2-TPR was performed in a quartz U-type tube quartz reactor using a TCD as detector. 100 mg sample was used and heated in O_2 at 450 °C for 1 h. Then the sample was cooled to 100 °C in O_2 flow (30 ml/min). The reducing gas was 5 vol.% H_2/Ar and its flow rate was 30 ml/min. The sample was heated at 10 °C/min from 100 to

750 °C. The CO_2-TPD was carried in the above equipment by an online MS (Hide HPR20), and the adsorption of CO_2 was performed at 100 °C.

2.3 Catalytic activity measurement

2.3.1 Catalytic oxidation of CO

The catalytic activity of CeO_2 catalysts towards CO oxidation was carried out in a continuous flow reactor. The catalyst particles (200 mg) were placed in the reactor, and treated for 2 h in O_2 flow (10 ml/min) at 400 °C. The reactant gases (1.0% CO, 16% O_2, balanced with Ar) went through the reactor at a rate of 50 ml/min. The initial catalytic activity was continuously measured with the reaction temperature rising from 50 °C to 400 °C at 5 °C/min. The composition of the gas exiting the reactor was monitored by an on line mass spectrometer (HIDEN HPR20).

2.3.2 Catalytic oxidation of 1, 2-dichloroethane

Catalytic oxidation of 1, 2-dichloroethane was carried out with 200 mg of catalyst (40-60 mesh) in a continuous flow micro-reactor constituted of a U-shaped quartz tube of 3 mm of inner diameter at atmospheric pressure. The gas stream was composed of 450 ppm of 1, 2-dichloroethane and air in 50 cm^3/min (GHSV = 15,000 h^{-1}). The reaction was run from 100 to 250 °C in a step mode with a 15 min plateau at each temperature investigated. The effluent gases were analyzed by an on-line gas chromatograph equipped with a flame ionization detector (FID).

3. RESULTS AND DISCUSSION

3.1 Synthesis of CeO_2 nanosheets

The morphology of the final products synthesized at different temperatures (aging for 15 h) was observed by SEM (Figure 1a-f). As shown in Figure 1, when the reaction temperature was below 75 °C, the obtained products displayed obvious sheet-like morphology and the thickness of sheets was about 20-50 nm. However, some distinct differences among these nanosheets can still be observed. For instances, the nanosheets obtained at 0 °C were petal-like and self assembled into flower-like structure, by contrast, the product achieved at 25 °C was mainly consisted of uniform belt-like nanosheet with a length of about 5-10 μm and a width of about 0.5-1.2 μm. Additionally, the edges of belt-like nanosheets got rough and the shape also was non-uniform when the reaction temperature was increased to 50 °C. Further increasing the reaction temperature, the olive-like morphology was observed at 75 °C and 100 °C and composed by multilayer sheets. The magnified SEM images showed olive-like sheets were aggregated by CeO_2 nanoparticles. Be noted that, the sample obtained at 150 °C was prepared via a route of precipitation reaction at 100 °C and then hydrothermal treatment at 150 °C. Figure 1f demonstrated that the sample was mainly composed by irregular aggregated particles, however, the olive-like morphology can still be found (Figure S1). Therefore, it can be speculated that the dissolution-recrystallization process may be occurred at high temperature.

Figure 1

To investigate deeply the unexpected morphology evolvement and the occurring of dissolution-recrystallization process, the as-synthesized precursor at 0 °C was hydrothermally treated at high temperature (such as for 24 h at 150 °C or 170 °C) and SEM/TEM images were shown in Figure 2. After hydrothermal treatment of sheet-like precursor at high temperature and thermal decomposition, CeO_2 nanopolyhedra with the size of 200-300 nm were formed as shown in Figure 2b and Figure 2c, and the polyhedral nature of the nanoparticles was confirmed once again by TEM (Figure 2d). Furthermore, the process, including the first dissolution of sheet-like precursor and then the growth into nanopolyhedra via recrystallization, was observed visually due to the existence of part sheet-like structure (Figure 2b). Combining the above experimental results, it was reasonably believed that the lower reaction temperature was favor to the formation of sheet-like structure due to slow rate of crystalline growth and low dissolubility, however, the dissolution-recrystallization was dominant at higher temperature and finally grew into polyhedra structure.

Figure 2

Additionally, the crystal phase of as-synthesized precursors and calcined samples was investigated via XRD technique, and the corresponding XRD patterns were displayed in Figure 3. For all calcined samples (Figure 3b), all the detectable peaks in the pattern can be indexed to the pure cubic fluorite CeO_2 with a lattice constant a = 0.5414 nm (JCPDS 34-394). Using Debye-Scherrer formula, the strongest peaks (111)

at 2θ = 28.5 ° were used to calculate the average grain size of the CeO_2 particles, it was determined to be around 15-20 nm and increased with the increase of reaction temperature. No crystalline impurity was detected from the XRD spectra. However, the crystal phase of as-synthesized precursors (the uncalcined precipitates) at different temperatures was distinct. The as-synthesized samples at 0 °C and 25 °C showed an unknown phase, and the weak intensity of the pattern indicated that the samples had poor crystallinity, which was related to the low reaction temperature. When the reaction temperature was increased to 50 °C, diffraction peaks of orthorhombic cerium carbonate hydrate ($Ce_2(CO_3)_3$•$6H_2O$, JCPDS 30-295) were found in the XRD pattern and the intensity evidently increased, which indicated a good crystallinity. As the reaction temperature was further raised to 75 °C or more, the as-prepared samples showed the diffraction peaks of $CeOHCO_3$. It can be found that pure orthorhombic $CeOHCO_3$ (JCPDS 41-13) can be obtained at 75 °C and 100 °C, but hexagonal $CeOHCO_3$ (JCPDS 32-189) with a part of cubic fluorite CeO_2 phase (JCPDS 34-394) was formed at 150 °C. The details about phase of these precursors can be seen in Supporting Information (Figure S2). Additionally, it can be found that the crystal phase of the as-synthesized precursors transformed from the original unknown phase to $CeOHCO_3$ after the precursors prepared at 0 °C were hydrothermally treated at 150 °C and 170 °C (see Figure S2), but accompanied by a part of cubic fluorite CeO_2 phase. In detail, the precursors treated hydrothermally at 150 °C and 170 °C mainly exhibited the mixed crystal structure of orthorhombic and hexagonal $CeOHCO_3$ and the crystal structure of hexagonal $CeOHCO_3$, respectively, but the both accompanied

by a part of cubic fluorite CeO_2 phase. Generally, the $CeOHCO_3$ crystal exhibits two important phases, i.e., orthorhombic and hexagonal phase. The orthorhombic phase is more stable than its hexagonal phase, and the stable structure phase with lower nucleation barrier is preferred to emerge according to the free energy and Ostwald step rule. Thus, our results were consistent with the common idea that orthorhombic $CeOHCO_3$ is the stable phase and it is difficult to get pure hexagonal $CeOHCO_3$ under mild conditions. Han [20] previously reported that orthorhombic $CeOHCO_3$ crystals with good crystallinity could be prepared at 160 °C, and the hexagonal phase was formed only with the further increase of temperature and reaction period. Their results showed that suitably higher temperature and longer time were favorable to the growth of hexagonal $CeOHCO_3$ crystals.

Figure 3

More characteristics of the precursors were also investigated in its FT-IR spectra (Figure 4). For the precursor obtained at 150 °C, the band centered at 3476 cm^{-1} was ascribed to the O-H stretching vibration in OH^- group, and the 3620 cm^{-1} band was normally attributed to O-H bending vibrations combined with Ce atoms. The intensive peaks at 1510 and 1443 cm^{-1} were assigned to the υ_3 mode of CO_3^{2-} group, and the peaks at the 872 and 712 cm^{-1} were assigned to the υ_2 and υ_4 modes of the CO_3^{2-} group, respectively. The peaks at 600 and 782 cm^{-1} were also due to the vibration of the CO_3^{2-} group. The minor peaks in 2000-3000 cm^{-1} were assigned to C-H vibrations. The absorption bands agreed with the ones previously reported in the literature, which

was characteristic peaks of hexagonal structure $CeOHCO_3$ [21]. The FT-IR spectra of the precursors obtained at 75 and 100 °C were same, which was in good agreement with the results of XRD showing the both were orthorhombic $CeOHCO_3$. Apparently, peaks of the precursors obtained at 0, 25 and 50 °C were different with above three samples, but these three precursors demonstrated same characteristic peaks and the characteristic peaks of OH^- group disappeared. The strong absorption band between 1300 and 1600 cm^{-1} was due to carbonate ion stretching vibration, the sharp absorption peaks between 600 and 900 cm^{-1} were due to carbonate ion bending vibration, and the absorption band between 3000 and 3750 cm^{-1} was due to -OH group of H_2O. These proved that the precursor was hydrated cerium carbonate ($Ce_2(CO_3)_3 \cdot xH_2O$), not the mixed salts of cerium and ammonium carbonates [22]. Additionally, according to the XRD results, the precursor obtained at 50 °C showed a single phase of orthorhombic cerium carbonate hydrate ($Ce_2(CO_3)_3 \cdot 6H_2O$), thus, it was speculated that the precursors obtained at 0 and 25 °C may be a sort of cerium carbonate hydrate with poor crystallinity.

Figure 4

Previously, a few literatures [10, 11, 23, 24] reported that sheet-like CeO_2 could be synthesized via controlling the morphology of $Ce(OH)CO_3$ precursors, and it was widely thought that the crystal phase of $Ce(OH)CO_3$, hexagonal or orthorhombic phase, was crucial. However, in our work, it was found that the petal/belt-like CeO_2 nanosheets could be obtained by the calcination of $Ce_2(CO_3)_3$ precursors with

corresponding morphologies, while the morphology of precursors (petal or belt-like) was determined by controlling reaction temperature. For instance, limitation of the crystalline growth at low temperature (0 °C) resulted in the formation of petal-like $Ce_2(CO_3)_3$ precursor, and the higher temperature (25 °C) was favor to the the growth of crystalline along a specific direction and generated belt-like $Ce_2(CO_3)_3$ precursor. In order to explore the effect of as-synthesized precursor, the different precipitants, such as aqueous ammonia (AA), sodium bicarbonate (SB), ammonium carbonate (AC) and sodium carbonate (SC), were investigated at 0 °C.

As shown in Figure 5, sheet-like CeO_2 could be synthesized using SB, AC and SC as precipitants with the exception of AA (the detail SEM images can be seen in Figure S3). Among these sheet-like morphologies, the sample prepared using SB as precipitant exhibited a similar petal-like sheet with the sample obtained using ammonium bicarbonate as precipitant, while AC and SC as precipitants, plate-like CeO_2 could be formed and was similar with the reports of Yin [25]. Moreover, Figure 5e showed the XRD patterns of prepared precursors. The peaks of samples synthesized using AA and SC as precipitants could be indexed as the single phase of cubic fluorite CeO_2 and orthorhombic cerium carbonate hydrate ($Ce_2(CO_3)_3 \cdot 6H_2O$, JCPDS 30-295), respectively. While SB and AC as precipitants, the obtained precursors were of unknown phase, but may be cerium carbonate hydrate, which was same with that of ammonium bicarbonate as precipitant at 0 °C and 25 °C.

Figure 5

Phase of as-synthesized precursors and morphologies of CeO_2 at different temperatures and using different precipitants were summarized in Table 1. In our synthesis system, the possible reaction process as follows:

$$HCO_3^-(aq) + H_2O \rightleftharpoons H_2CO_3(aq) + OH^- \quad (1)$$

$$Ce^{3+}(aq) + OH^-(aq) \rightleftharpoons CeOH^{2+}(aq) \quad (2)$$

$$CeOH^{2+}(aq) + CO_3^{2-}(aq) \longrightarrow CeOHCO_3(s) \quad (3)$$

$$2Ce^{3+}(aq) + 3CO_3^{2-}(aq) \longrightarrow Ce_2(CO_3)_3(s) \quad (4)$$

For the formation of $CeOHCO_3$, trivalent Ce^{3+} had strong affinity for OH^-, and formed the $Ce(OH)^{2+}$ polyatomic group. At elevated temperature, CO_3^{2-} tends to bond with the positive-charged groups to yield solid $CeOHCO_3$ at high supersaturation [26]. However, our results showed that the formation of $Ce_2(CO_3)_3$ was more favorable at lower temperature, which may be associated with low concentration of OH^-.

Thus it can be seen that, the two kinds of cerium carbonate hydrate precursors ($Ce_2(CO_3)_3 \cdot 6H_2O$ and $Ce_2(CO_3)_3 \cdot xH_2O$) both formed sheet-like structure at lower temperature and then transformed into CeO_2 via a calcination process, but the detail morphologies, such as plate-like, belt-like or petal-like, was not related with the crystal phase and the reason was still not clear. Whereas, the $Ce(OH)CO_3$ precursors obtained only at higher temperature presented irregular particle-like or polyhedral morphologies due to the dissolution-recrystallization and Ostwald ripening processes.

Table 1

Many experimental parameters such as aging time, amount of water and adding

way of precipitant at 0 °C were investigated. The SEM images (Figure S4) showed that CeO_2 nanosheets could be formed even without aging, and the aging time more greatly effected the thickness of nanosheets, increasing from 30-50 nm to 70-100 nm (after aging for 48 h). Thus, except stated otherwise, the following all samples were aged for 24 h. Additionally, even amount of water decreased from 400 ml to 100 ml or 50 ml, flower-like CeO_2 from self-assembly of petal-like nanosheets at 0 °C still could be synthesized, and the belt-like nanosheets also could be obtained (Figure S5). However, when ammonium bicarbonate precipitant was added into cerium nitrate solution by slowly dropping way (2.5ml/min), the obtained CeO_2 displayed an aggregative structure in a rod-like particles, and the precursor exhibited orthorhombic cerium carbonate hydrate ($Ce_2(CO_3)_3 \cdot 8\ H_2O$, JCPDS 38-377) phase (Figure 5f, Figure S6 and Figure S7). Therefore, it is speculated that high supersaturation was a key factor for preparing sheet-like CeO_2 via phase transformation of high anisotropic precursors, such as $Ce_2(CO_3)_3$, and $CeOHCO_3$.

On the basis of the experimental results, a possible growth process demonstrating the synthesis of CeO_2 with different morphologies can be simply described in Figure 6.

Figure 6

3.2 Characterization of petal- and belt-like CeO_2 nanosheets

More detailed structural information about the petal- and belt-like CeO_2 nanosheets was further provided by High-resolution TEM (HRTEM). Figure 7a and 7d show the

magnified image of the CeO_2 samples aged for 24 h at 0 °C and 25 °C, it further indicated that the both CeO_2 samples were sheet-like structure. Figure 7b and 7e further display that each nanosheet was composed of numerous densely packed particles, and it was the particles and their interspacing voids that were responsible for the roughness, which was similar with the reports of Deng [12]. Figure 7c and 7f directly showed that the lattice spacing was 0.30 nm, close to the (111) lattice spacing of the cubic phase of CeO_2. This result indicated that the exposed facets of the both nanosheets are (111) facets. Additionally, the corresponding selected area electron diffraction (SAED) pattern (Figure 7c and 7f) indicated that the CeO_2 nanosheets both are polycrystal structure with some defects.

Figure 7

Figure 8 showed the H_2-TPR and CO_2-TPD results of the two types of CeO_2 nanosheets, compared with the CeO_2 nanoparticles prepared by thermal decomposition method (CeO_2-TD). The petal-like (CeO_2-0) and belt-like CeO_2 (CeO_2-25) nanosheets both exhibited a broad peak between 300 and 550 °C centered at 500 °C that was attributed to less reactive surface oxygen species, and the hydrogen consumption of CeO_2-25 sample was slightly higher than that of CeO_2-0. The reduction above 750 °C was related to the reduction of lattice oxygen. For the CeO_2-TD sample, there are two overlapping peaks centered at 420 and 520 °C, respectively. By contrast, the reduction properties (such as oxygen mobility and oxygen storage capacity) of CeO_2 nanosheets are not superior to the CeO_2-TD sample.

As shown in Figure 8b, three samples displayed two peaks of CO_2 desorption at low temperature range, one at 150-170 °C, corresponding to the weak basic sites, another with the maximum at about 330 °C, associated with medium-strength basicity. Additionally, the amount of base sites of CeO_2-25 was obvious greater than that of CeO_2-0 and CeO_2-TD samples, which probably came from the larger surface areas and more number of defects in the framework of the CeO_2-25 sample, i.e. the number of oxygen atoms associated with Ce exhibiting a low coordination number.

Figure 8

3.3 Catalytic oxidation of CO

The catalytic CO oxidation performances of synthesized CeO_2 nanosheets and CeO_2 nanoparticles prepared by thermal decomposition method were shown in Figure 9. CeO_2 nanosheets (petal-like CeO_2-0 and belt-like CeO_2-25) exhibited higher conversion than CeO_2 nanoparticles prepared by thermal decomposition method, but CeO_2-25 sample was slightly better, especially at higher temperature. However, the catalytic activity was not directly related to the reduction properties of CeO_2 displayed in Figure 9a, which showed the CeO_2-TD could be reduced at lower temperature. Therefore, it can be considered that the enhanced catalytic activity could be attributed to their higher specific surface area, and the BET surface area of CeO_2-25 and CeO_2-0 was 68 cm^2/g and 15 cm^2/g, but the CeO_2-TD (45 cm^2/g) did not show a better activity than CeO_2-0. Additionally, compared with CeO_2 nanoparticles, the CO_2 adsorbed on surface of the CeO_2 nanosheets from the complete oxidation of CO more easily desorbed (seen in Figure 8b) and the more base sites presented on CeO_2

nanosheets, which could be another more important reason.

Figure 9

3.4 Catalytic oxidation of 1, 2-dichloroethane

The light-off curves and stability tests at 250 °C of 1, 2-dichloroethane (DCE) catalytic oxidation recorded at constant GHSV (15,000 h^{-1}) and feed concentration (550 ppm in air) over different CeO_2 and vanadia supported CeO_2 catalysts were presented in Figure 10. Three pure CeO_2 catalysts revealed almost overlapping activity curves except that at 250 °C, and the conversions of DCE at 250 °C were 90%, 80% and 70% over CeO_2-25, CeO_2-0 and CeO_2-TD catalysts, respectively. Moreover, the stability tests at 250 °C showed the conversion over all pure CeO_2 catalysts sharply dropped to 20-40% within 300 min, by contrast, the decline of CeO_2-TD catalyst was more severe and the conversion fell to about 20% only after 150 min. Compared with pure CeO_2 catalysts, the catalytic activities of the CeO_2 catalysts supported 5%wt vanadia were improved obviously, especially 5%wt VO_x/CeO_2-25 and 5%wt VO_x/CeO_2-0, for example, the $T_{50\%}$ of 5%wt VO_x/CeO_2-25 decreased from 210 °C to 175 °C and $T_{90\%}$ reduced from 250 °C to 225 °C. Moreover, the two kind of nanosheets supported catalysts also exhibited an almost same activity, being consistent with the results of pure CeO_2 catalysts, but a remarkable higher conversion than nanoparticles catalyst. The difference of catalytic activities between vanadia supported on CeO_2 nanosheets and nanoparticles may be from the high dispersion of vanadia on CeO_2 nanosheet due to its large surface areas and the easier dispersion

over sheet-like CeO_2 than that particle-like CeO_2, which was favor to the expose of surface active sites of CeO_2, because CeO_2 is considered as the main active components for the catalytic combustion of chlorinated organic compounds over CeO_2 based catalysts [27]. Additionally, the stability tests at 250 °C showed that the CeO_2 nanosheets supported vanadia both presented a better stability, the conversion of DCE decreased from 97% to 92% in the last 40 min and then maintained stable for at least 400 min. Similar with the pure CeO_2 catalysts, the decline of VO_x/CeO_2-TD catalyst was greater, from 86% to 62%. Thus it can be seen, the loading of vanadia apparently improved the stability of CeO_2 (whether sheet-like CeO_2 or traditional CeO_2 particle) for catalytic oxidation of DCE.

More importantly, large amounts of vinyl chloride (VC) could be detected over all pure CeO_2 catalysts, while only trace of VC was observed over vanadia supported catalysts. Vinyl chloride, usually as intermediate was found during the catalytic oxidation of DCE over HZSM-5 solid acid catalysts, being stable, does not undergo further dehydrochlorination and oxidized to CO, CO_2 and HCl even at 400 °C [28], due to the absence of oxidative active sites over the solid acid catalysts. Thus, the presence of VC suggested that the abstraction of HCl (dehydrochlorination) also was the first step for the catalytic oxidation of DCE over the CeO_2 based catalysts. Furthermore, CeO_2 supported vanadia catalysts possessed more excellent oxidation performance compared with pure CeO_2, the H_2-TPR profiles of VO_x/CeO_2 catalysts was listed in Figure 11, which contributed to the complete oxidation of VC intermediate into CO_2 and HCl.

Figure 10

Figure 11

4. CONCLUSIONS

In summary, petal-like and belt-like CeO_2 nanosheets have been synthesized by an aqueous phase precipitation method and NH_4HCO_3 as precipitant. In this procedure, any organic solvent and template or surfactant was not required, moreover, the preparing conditions were very mild and reaction temperature varied from 0 °C to 25 °C without hydrothermal or solvothermal treatment. The reaction temperature and supersaturation played key roles in the formation of ceria nanosheets, namely, lower temperature and higher supersaturation were favorable to the synthesis of sheet-like cerium carbonate hydrate by oriented aggregation process, whereas the elevated temperature could cause the dissolution-recrystallization and Ostwald ripening of precursors and then formed polyhedral CeO_2 by a thermal decomposition process. Additionally, compared with traditional CeO_2 nanoparticles, the pure ceria nanosheets and supported vanadia showed more excellent catalytic oxidation activities for catalytic oxidation of CO and 1, 2-dichloroethane. Especially, the VO_x/CeO_2 nanosheets showed a very promising application in the catalytic combustion of chlorinated volatile organic compounds (CVOCs). The findings of this work not only provided a simple means to achieve control of the morphology (from sheet-like to polyhedron) but also demonstrated that the catalytic oxidation performances can be enhanced by the variation of CeO_2 morphology.

ACKNOWLEDGMENTS

This research was supported by National Natural Science Foundation of China (Nos.21307033, 21277047), National Basic Research Program of China (Nos. 2010CB732300, 2011AA03A406), Shanghai Natural Science Foundation (No. 13ZR1411000), Commission of Science and Technology of Shanghai Municipality (No. 11JC1402900), Development Program for Young Teachers in Shanghai Universities and the Opening Project of Key Laboratory of Nuclear Radiation and Nuclear Energy Technology, Chinese Academy of Sciences (NRNE-OP2012001).

REFERENCES

[1] K. B. Zhou, X. Wang, X. M. Sun, Q. Peng, Y. D. Li, *J. Catal.* 2005, **229**, 206-212.

[2] Z. Y. Sun, H. Y. Zhang, G. M. An, G. Y. Yang, Z. M. Liu, *J. Mater. Chem.* 2010, **20**, 1947-1952.

[3] W. Q. Han, L. J. Wu, Y. M. Zhu, *J. Am. Chem. Soc.* 2005, **127**, 12814-12815.

[4] C. Ho, J. C. Yu, T. Kwong, A. C. Mak, S. Lai, *Chem. Mater*. 2005, **17**, 4514-4522.

[5] H. F. Li, G. Z. Lu, Q. G. Dai, Y. Q. Wang, Y. Guo, Y. L. Guo, *ACS Appl. Mater. Interfaces* 2010, **2**, 838-846.

[6] Z. Y. Huo, C. Chen, X. W. Liu, D. R. Chu, H. H. Li, Q. Peng, Y. D. Li, *Chem. Commun*. 2008, **32**, 3741-3743.

[7] J. J. Wei, Z. J. Yang, Y. Z. Yang, *CrystEngComm*. 2011, **13**, 2418-2424.

[8] K. S. Novoselov, A. K. Geim, S. V. Morozov, D. Jiang, Y. Zhang, S. V. Dubonos, I. V. Grigorieva, A. A. Firsov, *Science* 2004, **306**, 666-669.

[9] M. Choi, K. Na, J. Kim, Y. Sakamoto, O. Terasaki, R. Ryoo, *Nature* 2009, **461**, 246-249.

[10] C.R. Li, Q. T. Sun, N. P. Lu, B. Y. Chen, W. J. Dong, *J. Cryst. Growth*. 2012, **343**, 95-100.

[11] Y. F. Yu, Y. M. Zhu, M. Meng, *Dalton Trans*. 2013, **42**, 12087-12092.

[12] W. Deng, X. Y. Wang, F. Jiao, K. K. Zhu, *J. Nanopart. Res*. 2013, **15**, 1944-1953.

[13] B. Liu, Q. J. Li, X. B. Du, B. B. Liu, M. G. Yao, Z. P. Li, R. Liu, D. D. Liu, X. Zou, H. Lv, D. M. Li, B. Zou, T. Cui, G. T. Zou, *J. Alloys Compd*. 2011, **509**, 6720-6724.

[14] R. C. Rao, M. Yang, Q. Ling, Q. Y. Zhang, H. D. Liu, A. M. Zhang, W. Chen, *Micropor. Mesopor. Mater*. 2013, **169**, 81-87.

[15] Y. F. Sun, Q. H. Liu, S. Gao, H. Cheng, F. C. Lei, Z. H. Sun, Y. Jiang, H. B. Su, S. Q. Wei, Y. Xie, *Nat. Commun*. 2013, **4**, 2899-2907.

[16] T. Yu, B. Lim, Y. N. Xia, *Angew. Chem. Int. Ed*. 2010, **49**, 4484-4487.

[17] Y. Minamidate, S. Yin, T. Sato, *Mater. Chem. Phys*. 2010, **123**, 516-520.

[18] X. G. Han, L. Li, C. Wang, *CrystEngComm.* 2012, **14**, 1939-1941.

[19] X. Wang, D. P. Liu, S. Y. Song, L. Zeng, Y. Zhang, *Dalton Trans*. 2012, **41**, 7193-7195.

[20] Z. H. Han, N. Guo, K. B. Tang, S. H. Yu, H. Q. Zhao, Y. T. Qian, *J. Cryst. Growth* 2000, **219**, 315-318.

[21] X. F. Shang, W. C. Lu, B. H. Yue, L. M. Zhang, J. P. Ni, Y. lv, Y. L. Feng, *Cryst. Growth Des*. 2009, **9**, 1415-1420.

[22] Y. Q. Zhai, S. Y. Zhang, H. Pang, *Mater. Lett*. 2007, **61**, 1863-1866.

[23] S. F. Wang, F. Gu, C. Z. Li, H. M. Cao, *J. Cryst. Growth* 2007, **307**, 386-394.

[24] C. Fu, R. Li, Q. Tang, C. Q. Li, S. Yin, T. Sato, *Res Chem. Intermed*. 2011, **37**, 319-327.

[25] S. Yin, Y. Minamidate, S. Tonouchi, T. Goto, Q. Dong, H. Yamane, T. Sato, RSC Adv. 2012, **2**, 5976-5982.

[26] Z. H. Han, Y. T. Qian, S. H. Yu, K. B. Tang, H. Q. Zhao, N. Guo, *Inorg. Chem*. 2000, **39**, 4380-4392.

[27] Q. G. Dai, S.X. Bai, J. W. Wang, M. Li, X. Y. Wang, G. Z. Lu, *Appl. Catal. B: Environ*. 2013, **142**, 222-233.

[28] A. Aranzabal, J. A. González-Marcos, M. Romero-Sáez, J. R. González-Velasco, M. Guillemot, P. Magnoux, *Appl. Catal. B: Environ*. 2009, **88**, 533-541.

Table/ Figure Captions

Table 1 Phase of as-synthesized precursors and morphologies of CeO_2 at different temperatures and using different precipitants

Figure 1. SEM images of synthesized CeO_2 at different temperature (aging for 15 h): (a) 0 °C, (b) 25 °C, (c) 50 °C, (d) 75 °C, (e) 100 °C and (f) 150 °C.

Figure 2. SEM and TEM images of synthesized CeO_2: (a) as-synthesized precursor at 0 °C, (b) hydrothermally treated (a) sample at 150 °C, (c) hydrothermally treated (a) sample at 170 °C, (d) TEM of (c) sample.

Figure 3. XRD patterns of as-synthesized precursors (a) at different temperature and calcined samples (b).

Figure 4. FT-IR spectra of as-synthesized precursors at different temperature.

Figure 5. SEM images of samples prepared using different precipitants and XRD patterns of as-synthesized precursors: (a) aqueous ammonia (CeO_2-AA), (b) sodium bicarbonate (CeO_2-SB), (c) ammonium carbonate (CeO_2-AC), (d) sodium carbonate (CeO_2-SC), (e) XRD of a, b, c and d as-synthesized precursors, (f) ammonium bicarbonate as precipitant by slowly dropping way.

Figure 6. Schematic description of the growth process of CeO_2 with different morphologies.

Figure 7. HRTEM images of synthesized CeO_2 nanosheets prepared at 0 °C (a-c) and 25 °C (d-f).

Figure 8. H_2-TPR (a) and CO_2-TPD (b) profiles of CeO_2 nanosheets synthesized at 0 °C and 25 °C, and CeO_2 particles prepared by thermal decomposition method.

Figure 9. The catalytic performance of CeO_2 nanosheets for CO oxidation.

Figure 10. Light-off curves and stability tests of 1, 2-dichloroethane catalytic oxidation over CeO_2 and vanadia supported CeO_2 catalysts

Figure 11. H_2-TPR profiles of vanadia supported CeO_2 nanosheets and CeO_2 particles.

Table 1 Phase of as-synthesized precursors and morphologies of CeO_2 at different temperatures and using different precipitants

Properties	Temperature (°C, ammonium bicarbonate as precipitant)					
	0	25	50	75	100	150
Phase	$Ce_2(CO_3)_3$•xH_2O	$Ce_2(CO_3)_3$•xH_2O	*O*-$Ce_2(CO_3)_3$•$6H_2O$	*O*-Ce(OH)CO_3	*O*-Ce(OH)CO_3	*H*-Ce(OH)CO_3
Morphology	Petal-like	Belt-like	Irregular sheet	Olive-like	Olive-like	Irregular particles

Properties	Precipitants (at 0 °C)			
	$NaHCO_3$	$(NH_4)_2CO_3$	Na_2CO_3	NH_4HCO_3[a]
Phase	$Ce_2(CO_3)_3$•xH_2O	*O*-$Ce_2(CO_3)_3$•$6H_2O$	$Ce_2(CO_3)_3$•xH_2O	*O*-$Ce_2(CO_3)_3$•$8H_2O$
Morphology	Petal-like	Plate-like	Plate-like	Rod-like

[a] ammonium bicarbonate as precipitant by slowly dropping way

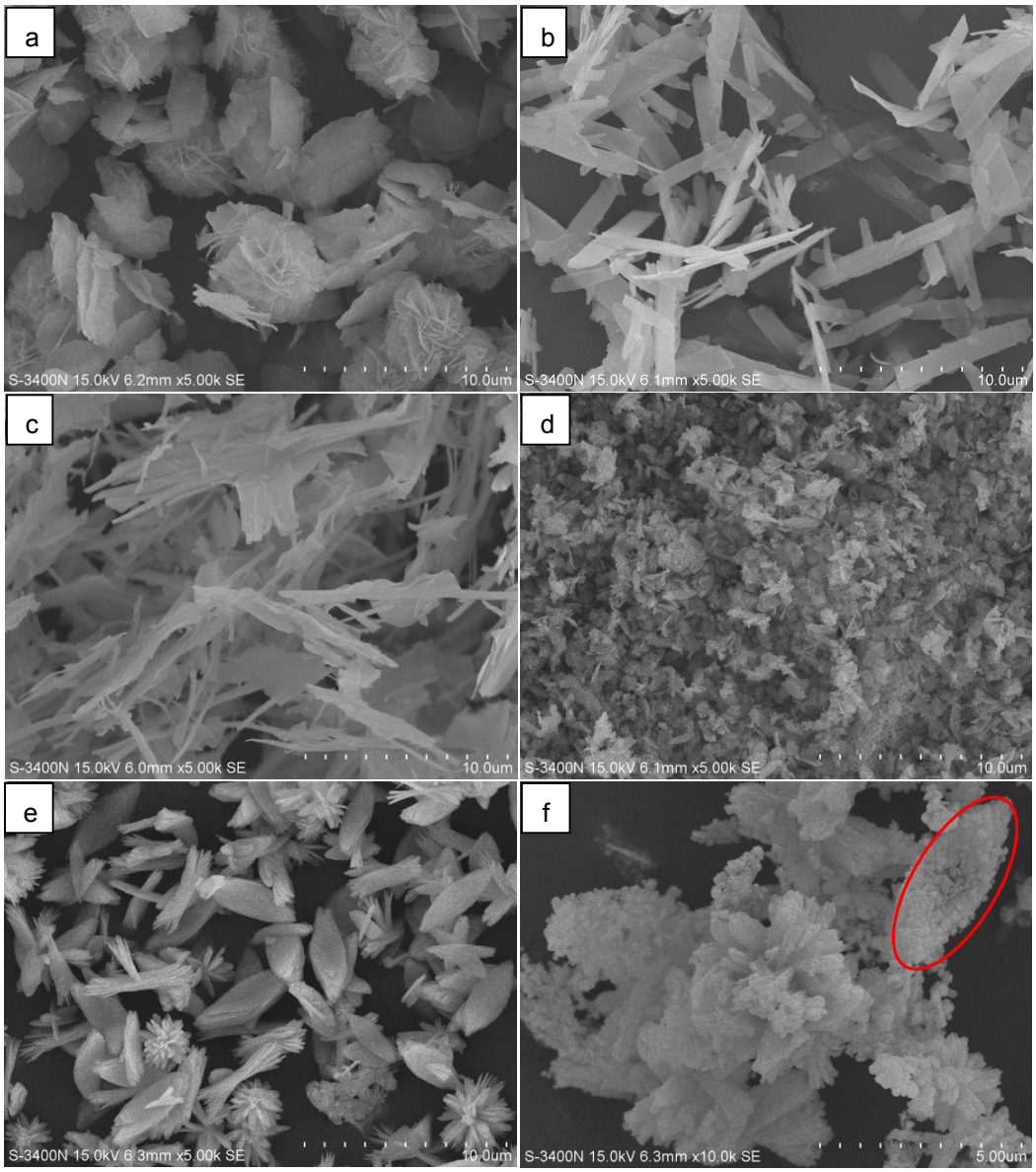

Figure 1. SEM images of synthesized CeO_2 at different temperature (aging for 15 h): (a) 0 °C, (b) 25 °C, (c) 50 °C, (d) 75 °C, (e) 100 °C and (f) 150 °C.

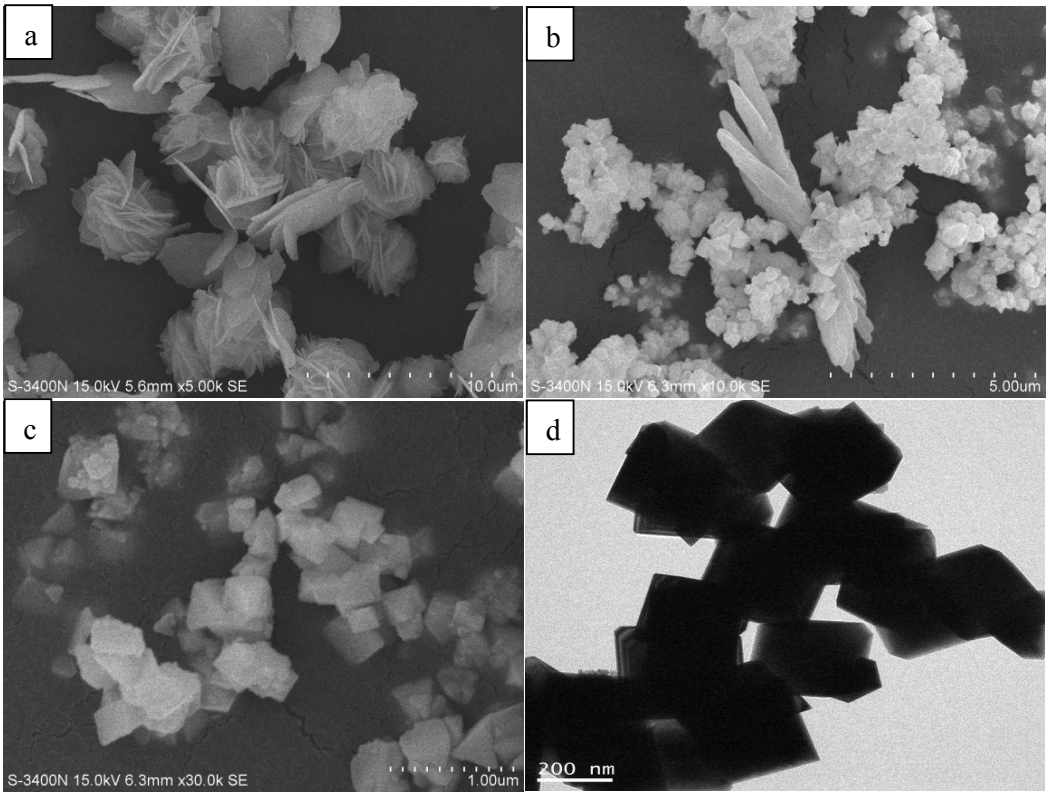

Figure 2. SEM and TEM images of synthesized CeO_2: (a) as-synthesized precursor at 0 °C, (b) hydrothermally treated (a) sample at 150 °C, (c) hydrothermally treated (a) sample at 170 °C, (d) TEM of (c) sample.

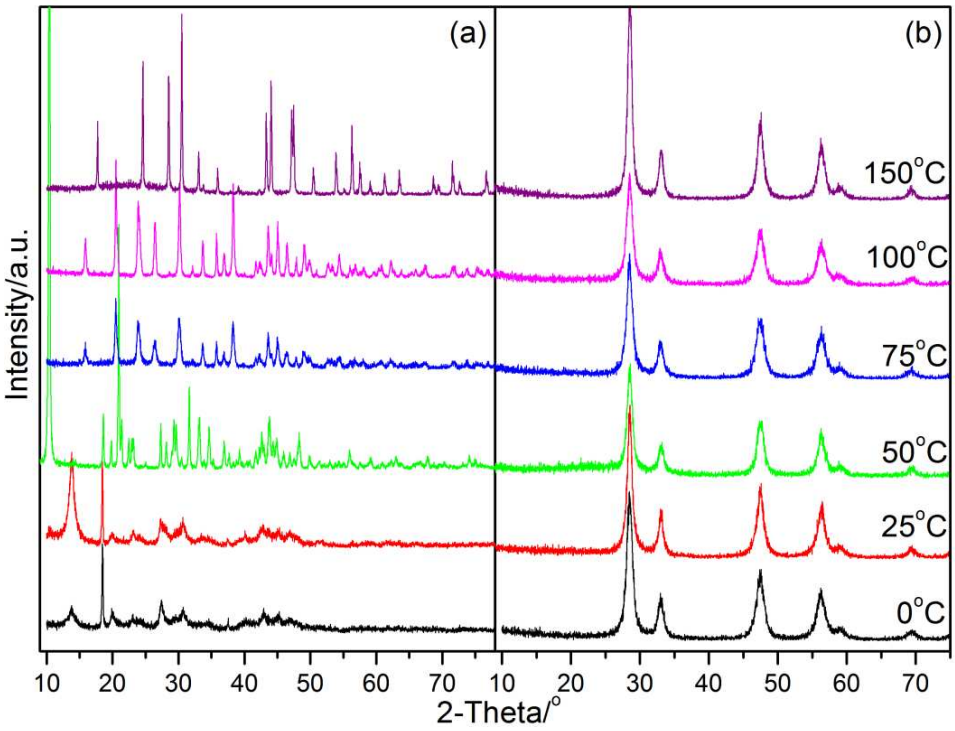

Figure 3. XRD patterns of as-synthesized precursors (a) at different temperature and calcined samples (b).

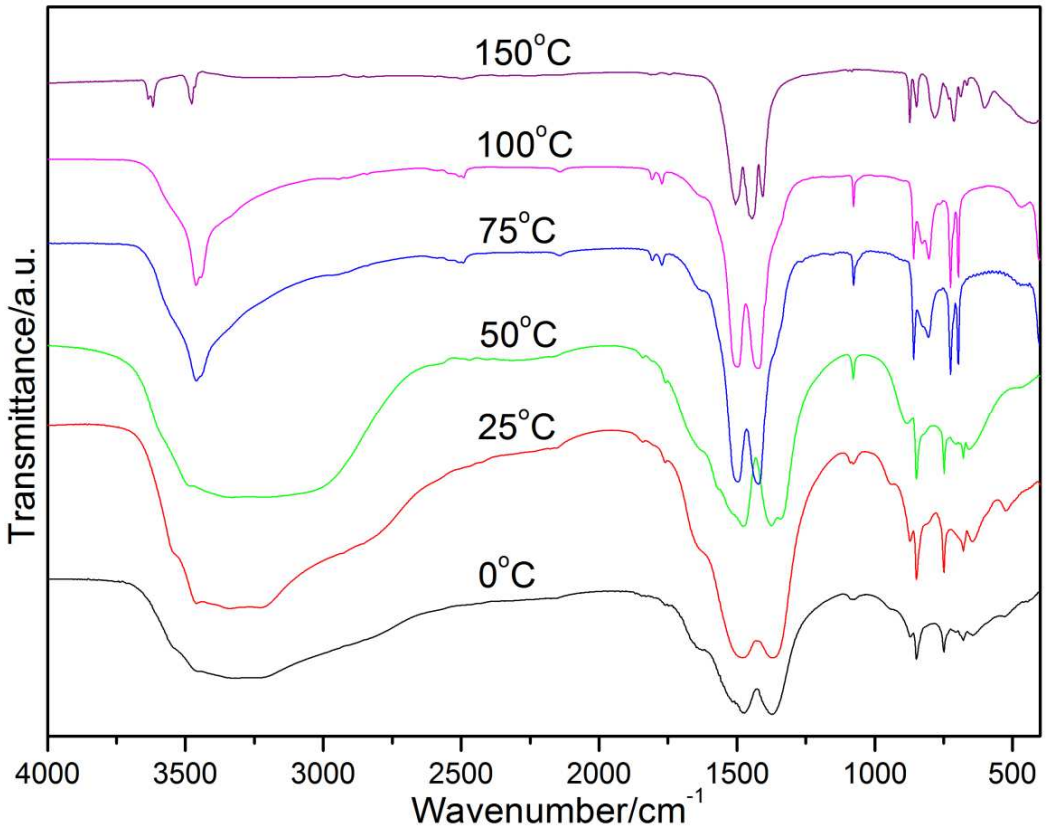

Figure 4. FT-IR spectra of as-synthesized precursors at different temperature.

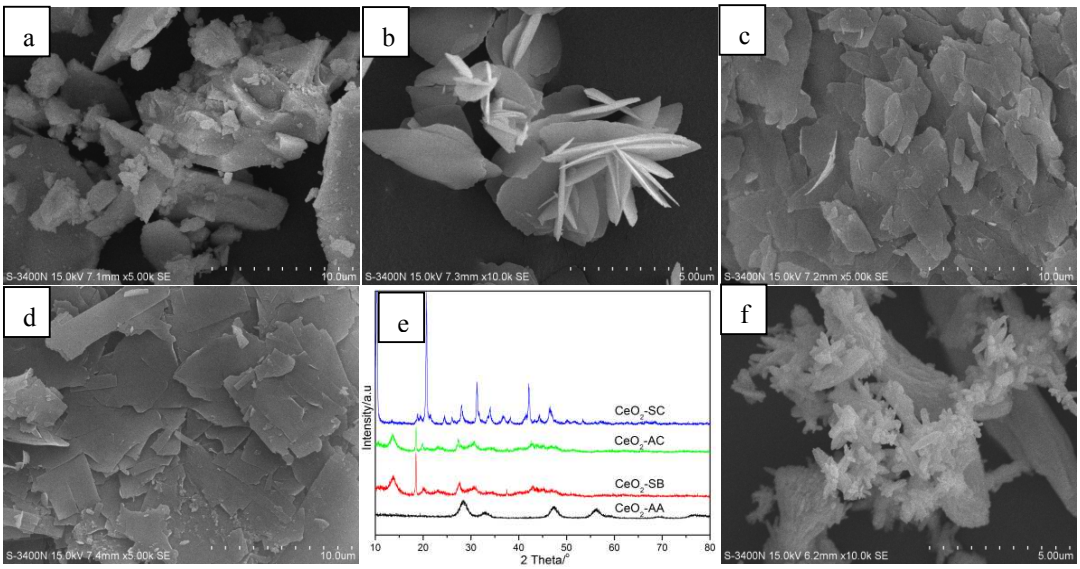

Figure 5. SEM images of samples prepared using different precipitants and XRD patterns of as-synthesized precursors: (a) aqueous ammonia (CeO_2-AA), (b) sodium bicarbonate (CeO_2-SB), (c) ammonium carbonate (CeO_2-AC), (d) sodium carbonate (CeO_2-SC), (e) XRD of a, b, c and d as-synthesized precursors, (f) ammonium bicarbonate as precipitant by slowly dropping way.

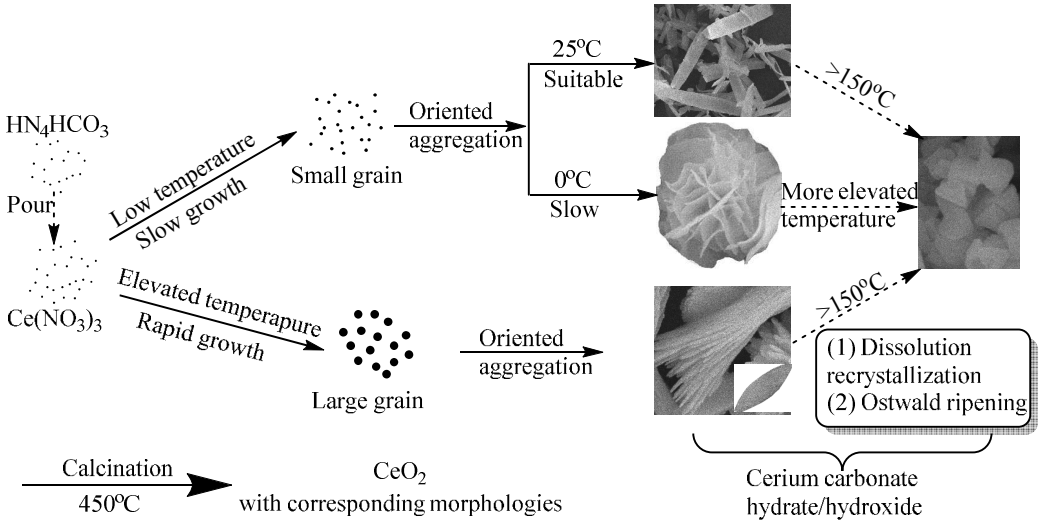

Figure 6. Schematic description of the growth process of CeO_2 with different morphologies.

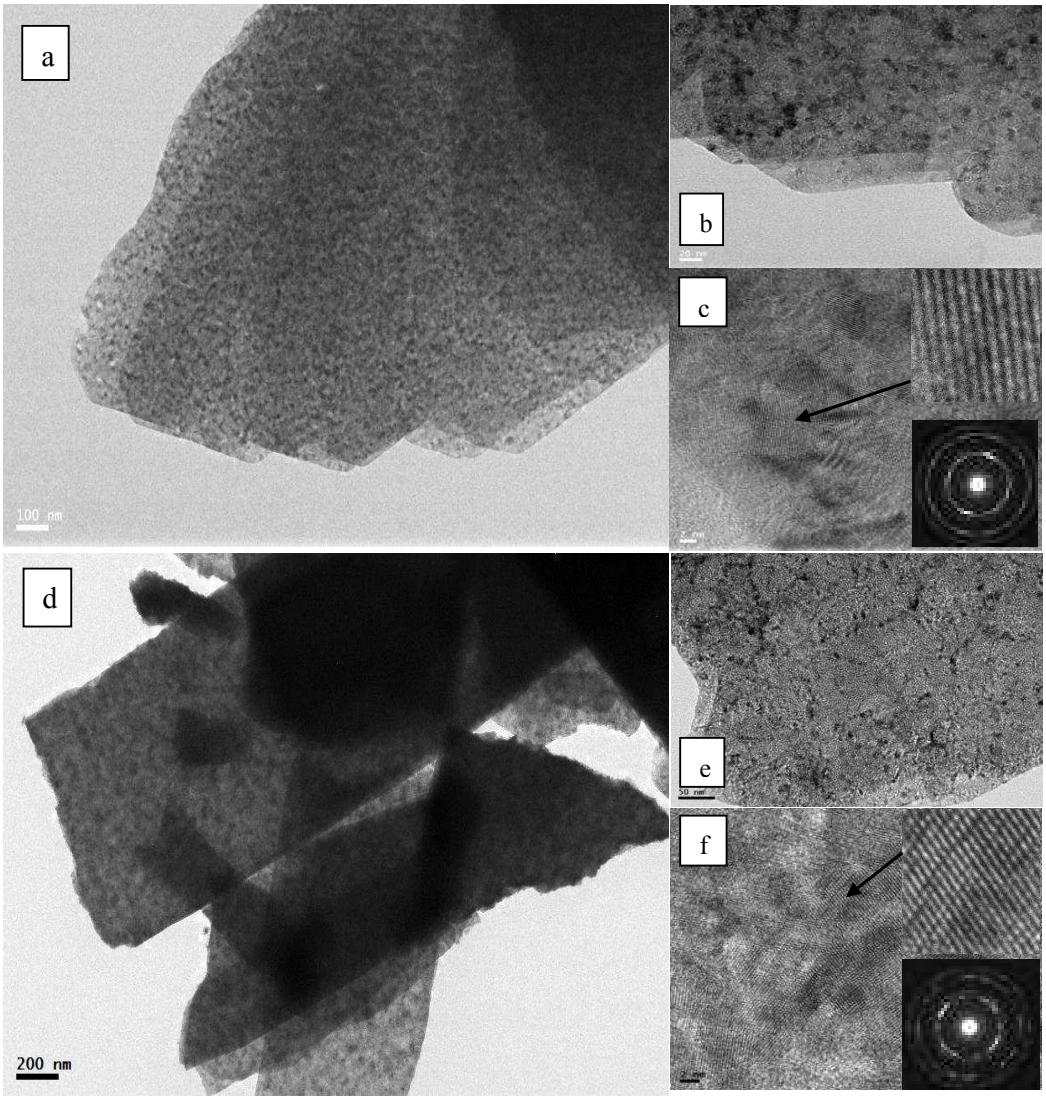

Figure 7. HRTEM images of synthesized CeO_2 nanosheets prepared at 0 °C (a-c) and 25 °C (d-f).

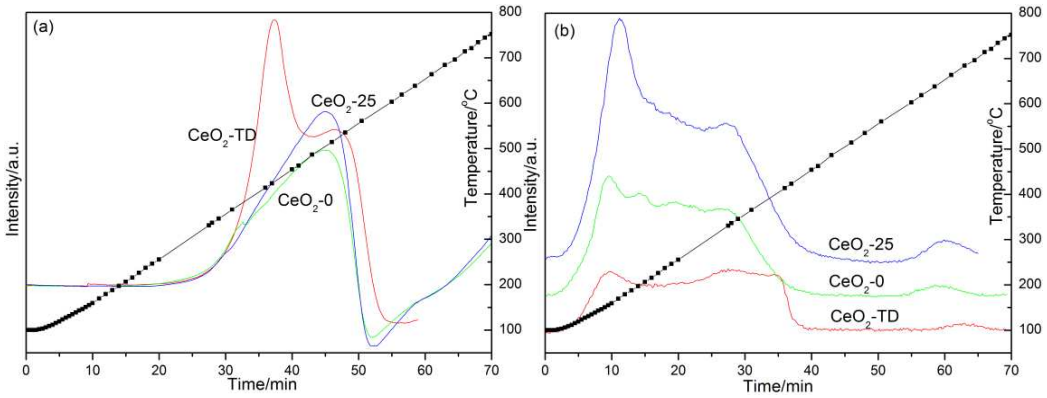

Figure 8. H_2-TPR (a) and CO_2-TPD (b) profiles of CeO_2 nanosheets synthesized at 0 °C and 25 °C, and CeO_2 particles prepared by thermal decomposition method.

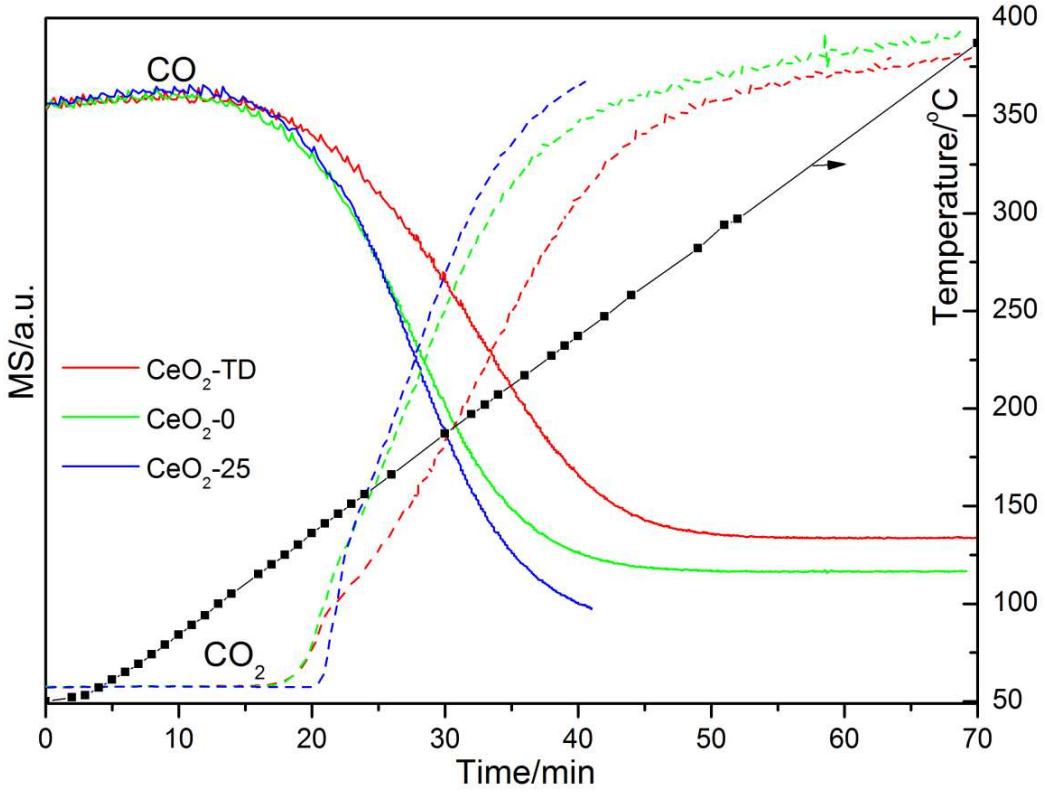

Figure 9. The catalytic performance of CeO_2 nanosheets for CO oxidation.

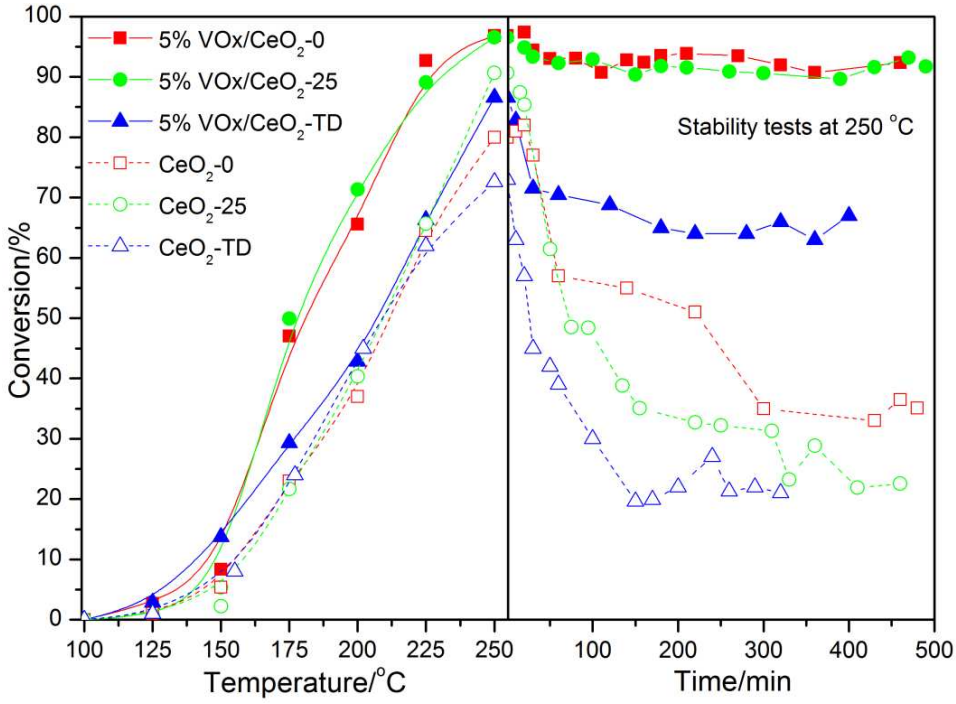

Figure 10. Light-off curves and stability tests of 1, 2-dichloroethane catalytic oxidation over CeO_2 and vanadia supported CeO_2 catalysts

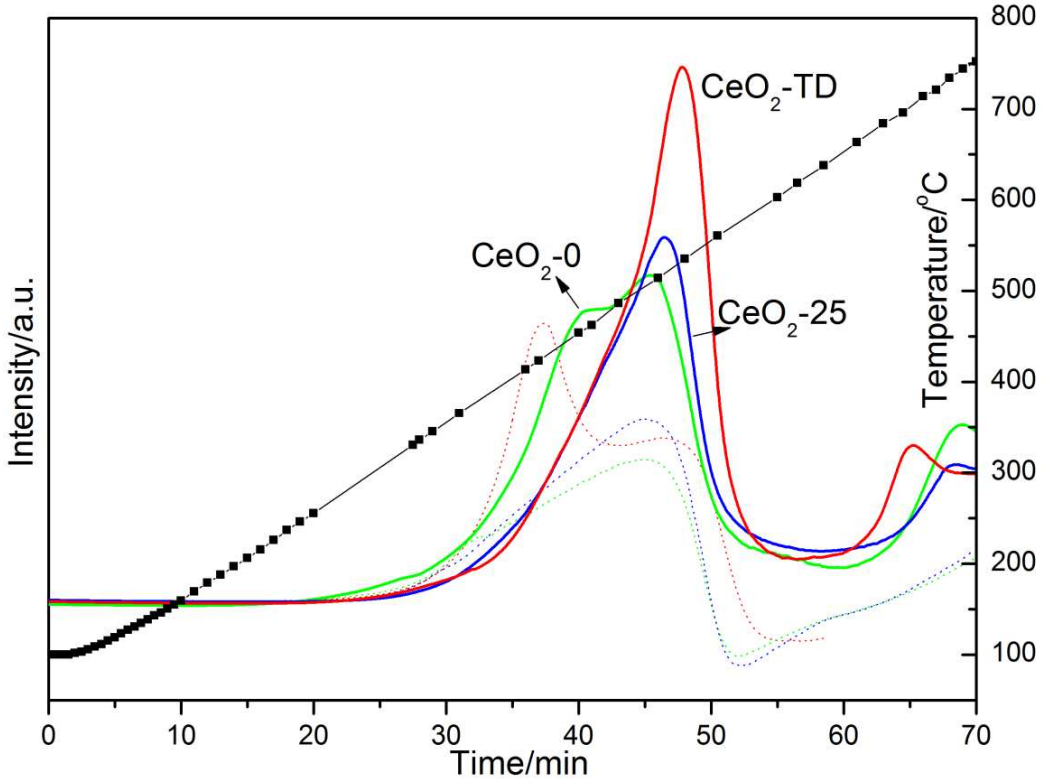

Figure 11. H_2-TPR profiles of vanadia supported CeO_2 nanosheets and CeO_2 particles.